REPORT DOCUMENTATION PAGE

Form Approved OMB No. 0704-0188

1. AGENCY USE ONLY (Leave blank)	2. REPORT DATE	3. REPORT TYPE AND DATES COVERED
	19 October 1999	Final Report

4. TITLE AND SUBTITLE

Increasing Microwave Output Power Pulselength in a 3 GW Backward Wave Oscillator Using Low-Energy Electron Beam-Treated Slow-Wave Structure Rings

5. FUNDING NUMBERS

F61775-98-WE080

6. AUTHOR(S)

Dr Sergei Korovin

7. PERFORMING ORGANIZATION NAME(S) AND ADDRESS(ES)

Institute of High Current Electronics
4 Akademicheskii Ave
Tomsk 634055
Russia

8. PERFORMING ORGANIZATION REPORT NUMBER

N/A

9. SPONSORING/MONITORING AGENCY NAME(S) AND ADDRESS(ES)

EOARD
PSC 802 BOX 14
FPO 09499-0200

10. SPONSORING/MONITORING AGENCY REPORT NUMBER

SPC 98-4024

11. SUPPLEMENTARY NOTES

12a. DISTRIBUTION/AVAILABILITY STATEMENT

Approved for public release; distribution is unlimited.

12b. DISTRIBUTION CODE

A

13. ABSTRACT (Maximum 200 words)

This report results from a contract tasking Institute of High Current Electronics as follows: The contractor will improve existing laboratory equipment to achieve the goal of extending microwave pulse duration to 40 nanoseconds using the SINUS-7 electron beam accelerator at the Institute of High Current Electronics as described in the proposal - final paragraph of the technical description excepted.

14. SUBJECT TERMS

EOARD, Pulsed Power, Electromagnetics

15. NUMBER OF PAGES

37

16. PRICE CODE

N/A

17. SECURITY CLASSIFICATION OF REPORT	18. SECURITY CLASSIFICATION OF THIS PAGE	19. SECURITY CLASSIFICATION OF ABSTRACT	20. LIMITATION OF ABSTRACT
UNCLASSIFIED	UNCLASSIFIED	UNCLASSIFIED	UL

INSTITUTE OF HIGH CURRENT ELECTRONICS
SIBERIAN DIVISION
RUSSIAN ACADEMY OF SCIENCES

Final Report

(Item 0003: 23 Nov 1998 - 22 May 1999)

Contract No. F61775-98-WE080

"INCREASING MICROWAVE OUTPUT POWER PULSELENGTH IN A 3-GW BACKWARD WAVE OSCILLATOR USING LOW-ENERGY ELECTRON BEAM - TREATED SLOW WAVE STRUCTURE RINGS"

_____ Dr. Sergei D. Korovin
Principal Investigator

_____ Dr. Dmitry I. Proskurovsky
Principal Investigator

Tomsk, Russia

CONTENTS

1. INTRODUCTION

In the relativistic microwave generators fed by high-current relativistic electron beams, the width of microwave pulse usually is limited to $10^{-8} \div 10^{-7}$ s while the electric field strength on the surface of the electrodynamic structure ranges $10^5 \div 10^6$ V/cm [1 - 4]. Herewith, with the growing of radiated power the pulse width decreases so that its energy stays approximately constant. At present, the maximum energy in microwave pulses of relativistic generators does not exceed several hundreds Joules. The circle of possible reasons of this phenomenon is sufficiently wide [4 - 9]. For Cherenkov devices with guiding magnetic field, at a pulse width of ~10 ns, when the motion of cathode and collector plasmas is small, the main role in the pulse shortening is probably plaid by plasma forming on the slow wave structure (SWS) in the intensive RF electric field. The possible sources of plasma are explosive-emission centers, as well as desrobed gas ionized by secondary-emission and scattered electrons.

The goal of the Contract is to demonstrate microwave pulse lengthening in the X-band relativistic Backward Wave Oscillator (BWO) with 3 GW peak output power using low energy high current electron beam (LEHCEB) treatment of BWO slow wave structure parts. In earlier experiments, the microwave pulse duration of the BWO at this power level ranged 6 nanoseconds only [3].

2. PULSED ELECTRON BEAM TREATMENT OF BWO SLOW-WAVE STRUCTURE PARTS

2.1. Formulation of Problem and Possible Solutions

To the date, a series of electrode preparation methods exists aimed at elimination of emitting points and improving the electric strength of vacuum insulation [10, 11]. As a rule, these methods do not allow maximum smoothing of surface simultaneously with efficient cleaning of surface layer from admixtures and contamination. At the same time, these methods are expensive and labor consuming.

We have developed a new method for enhancement of the electric strength of a vacuum insulation [12 - 14]. It is based on pretreatment of the electrode surface with a low-energy, high-current electron beam of microsecond duration. High energy density (10 J/cm^2 and more) and small pulse width of the electron beam allow the material surface layer treatment in the regime of melting as well as in the initial evaporation regime. Experiments have shown that this treatment substantially reduces the intensity of pre-breakdown currents and enhances the electric strength of the vacuum insulation. For instance, after LEHCEB treatment of stainless-steel

electrodes and subsequent conditioning of the vacuum gap with high-voltage pulses (250 kV, 40 ns, 100 pulses), the achieved breakdown electric field was 2.2 MV/cm.

However, it is not likely that the breakdown electric fields we obtained to the moment of Contract start are limiting. One of the most important reserves of improving the quality of vacuum insulation is the increase of cleanness in the process of electron-beam treatment. In experiments [12 - 15] an electron gun with plasma anode based on spark sources of carbon plasma and an explosive-emission graphite cathode was used (Fig. 1a). Besides, evacuation of the working chamber was made by means of an oil-vapor pump without catching out the oil vapor. Therefore, in course of electron beam treatment several amount of carbon containing (most dangerous) products of anode and cathode erosion and decay was coming onto the treated electrode surface that was decreasing the breakdown electric strength.

To reduce the flow of carbon containing contaminants onto the surface of slow wave structure under treatment we undertook the following:

1. Graphite cathode was replaced with a metal one;
2. Generally different method of anode plasma production was used;
3. The vacuum system was modernized to eliminate the oil vapors in the working chamber.

2.2. Modernized Electron-Beam Setup

We produced an electron gun where the anode plasma is generated in a pulsed reflected (Penning) discharge [16] (Fig. 1b). The e-beam collector and the explosive-emission cathode represent the Penning discharge cathodes. The anode is made as a ring whose inner diameter limits the diameter of the formed electron beam. External axial magnetic field serves for ignition of the reflected discharged and prevents the electron beam pinching during transportation.

The diagram of e-beam setup in Fig. 2. The cathode contains numerous thin copper wire emitters. The outer diameter of the cathode is 6 cm. The anode ring inner diameter was 7 or 10 cm and the width was 1 cm. The external guiding magnetic field (strength up to 3 kOe) is produced in a sectioned solenoid. The inlet of operating gas (Argon) is made stationary. Prior gas filling, the chamber is evacuated to $5*10^{-5}$ Torr using a diffusion pump. As a working liquid for the pump, the 5-phenyl-3-siloxan "• • -1" was used. In electric discharges, this liquid decays to elementary ephemeral hydrocarbons. In combination with ceramics filters installed in fore-vacuum channels this was providing sufficiently clean conditions for the treatment.

The discharge is initiated by applying a 5 kV, 200 μs pulse to anode. The discharge current is 55 A. The time delay for discharge ignition in the work diapason of pressures

p=(5 - 9)*10^{-4} Torr ranged 20-55 μs. As indicated by probe measurements, the concentration of plasma in the discharge was n_p≈(6 - 7)*10^{12} cm^{-3} with the electron temperature of ~5 eV [16].

The electron beam is produced as follows. In 10 – 20 μs after initiating the reflected discharge, a pulse of accelerating voltage with short rise time (not longer than 10 ns) is applied to the cathode. Experiments demonstrated that to efficiently excite the explosive emission on the cathode, accelerating voltage of 20-25 kV is sufficient. After development of explosive emission, the applied voltage is concentrated in a double electric layer between cathode and anode plasmas and here the electron beam is formed. Passing the anode opening, the beam is transported in plasma to the beam collector that holds the SWS part being treated.

Monitoring of accelerating voltage pulses was made using a resistive divider. The total circuit current and the collector current were measured by Rogowsky coil. The pass band for signal liners was not worse than 100 MHz and the error of measurement did not exceed 10%. The typical waveforms of diode voltage and beam current are represented in Fig. 3. As is seen, the energy spectrum of electrons is continuous, however, this fact does not substantially effect the distribution of energy deposition over the depth of material because the maximum pass depth for electrons is several times as less as the characteristic length for heat diffusion during the pulse [17].

The total energy of the electron beam was measured using a calorimeter based on calibrated thermoresistor KMT-8 and a copper absorber of special shape. The distribution of energy density over the beam cross section was measured by means of a sectioned calorimeter based on calibrated thermoresistors KTM-17 soldered to copper absorbers. The absorbers were made in the form of Faraday cylinders that allowed for measurements in the regime with notable evaporation of material since the bulk of evaporated material was dumping onto the internal lateral surface of the cylinder. To automatically control the measurements and improve its accuracy a special supporting circuit was employed connected to ADC. The accuracy of calorimetric measurements was not worse than 5 - 6 %

Fig. 4 illustrates a typical distribution of energy density over the e-beam cross-section $W(r)$ measured using a sectionalized calorimeter. As is seen, the distribution is uniform within a 5-cm spot that allows for simultaneous treatment of the entire target.

Experiments also demonstrated that the values of energy (energy density) obtained by means of integration of beam current and accelerating voltage waveforms agree with the results of calorimetric measurements to the accuracy of 10%. This indicates no substantial losses of beam kinetic energy during its transportation in plasma.

Sufficiently high (5 - 10 times) overcompensation of electron beam space charge gives it good stability in course of transportation to a distance of tens centimeters, despite the fact that the beam current is two orders larger then the limit Pierce current for this system [16].

2.3. Technique of SWS Parts Treatment

The diagram of e-beam treatment of BWO SWS part (corrugation rings and the beyond cutoff-neck) is represented in Fig. 2. The formed electron beam is passing though anode hole, transported in plasma to the collector and falls onto the SWS component under treatment. The component is fixed in manipulator that allows its rotation in vacuum. The angle of electron beam incidence with the respect to the component axis is 45 deg. The common view of the installation and operation chamber is represented in Fig. 5.

The order of SWS rings treatment was as follows. After machining, the rings were electrochemically polished in orto-phosphoric acid (H_3PO_4). Then the rings were flushed in distilled water and alcohol and placed in the chamber of the e-beam facility (one ring at once).

The e-beam irradiation of rings was made in two regimes consequently: first, at energy density of W=8 – 10 J/cm^2, then at W=5 – 6 J/cm^2. The electron beam pulse duration is τ=2.5 – 3 μs. Fig. 6 and Fig. 7 show the corresponding results of numerical simulation of heating regime. The simulation was made according to method [17]. As is seen, in the first case each pulse causes evaporation of ~0.4 μm surface layer and melting of ~4 μm layer while in the second case basically melting of surface layer of ~3 μm occurs without any substantial evaporation of the material (stainless steel). Thus, the first regime removes surface contamination and dissolved gas, the second one provides smoothing of micro relief.

Tuning of beam energy density was made by changing the charge voltage of the high voltage pulse generator as well as by changing the configuration and strength of guiding magnetic field.

To provide uniformity of treatment, each ring was exposed to 10 pulses, then it was turned at 30 deg for a new series of pulses. Then the procedure was repeating at lower energy density.

Since in course of treatment the temperature of rings was reaching 200 C, to prevent their oxidation, cooling of rings was made in Argon atmosphere at ~50 Torr during 20 – 30 minutes. After opening the chamber, treatment of the opposite side of ring was proceeding. The treatment of BWO cutoff-neck was made in similar manner.

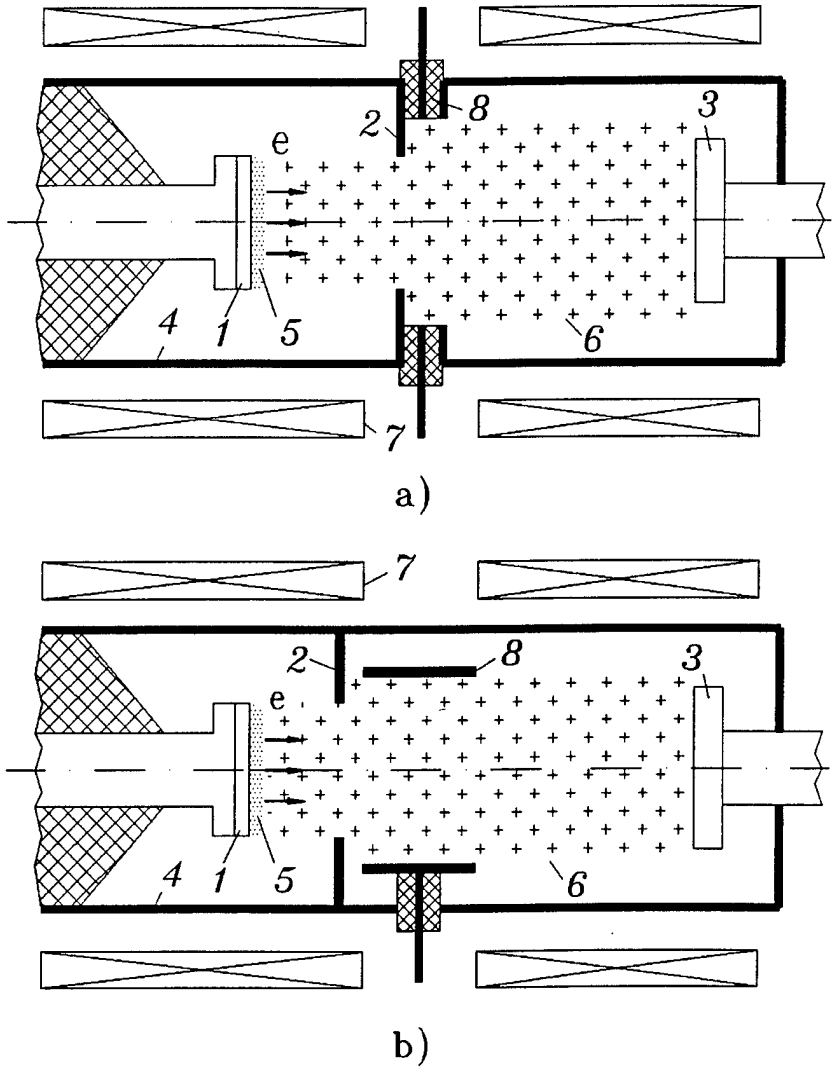

Fig. 1. Schematic diagrams of low-energy, high-current electron beam sources using plasma-filled systems based on vacuum spark plasma (a) and on gas discharge plasma (b): 1 - cathode, 2 - anode, 3 - collector, 4 - vacuum chamber, 5 - cathode plasma, 6 - anode plasma, 7 - solenoid, 8 - spark plasma sources (a) and the Penning cell anode (b).

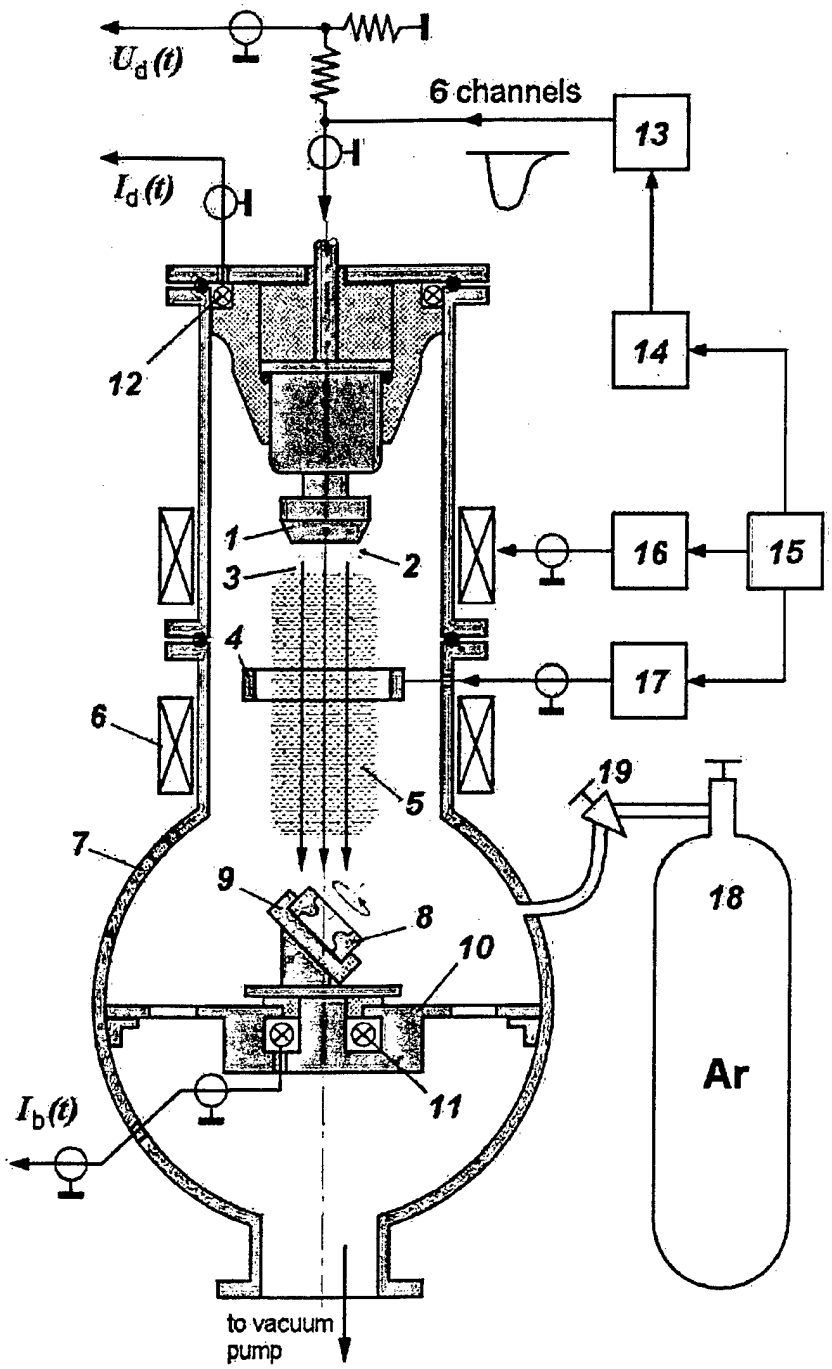

Fig. 2. Block diagram of the e-beam setup: 1 - cathode, 2 - explosive-emission cathode plasma, 3 - double electric layer, 4 - Penning cell cathode, 5 - gas-discharge anode plasma, 6 - solenoid, 7 - vacuum chamber, 8 - part (object) under treatment, 9 - manipulator, 10 - table, 11, 12 - Rogowsky coils, 13 - voltage pulse generator, 14 - starting unit for voltage pulse generator, 15 - control unit, 16 - solenoid power supply, 17 - Penning cell power supply, 18 - Ar vessel, 19 - leaker, R_1, R_2 - voltage divider.

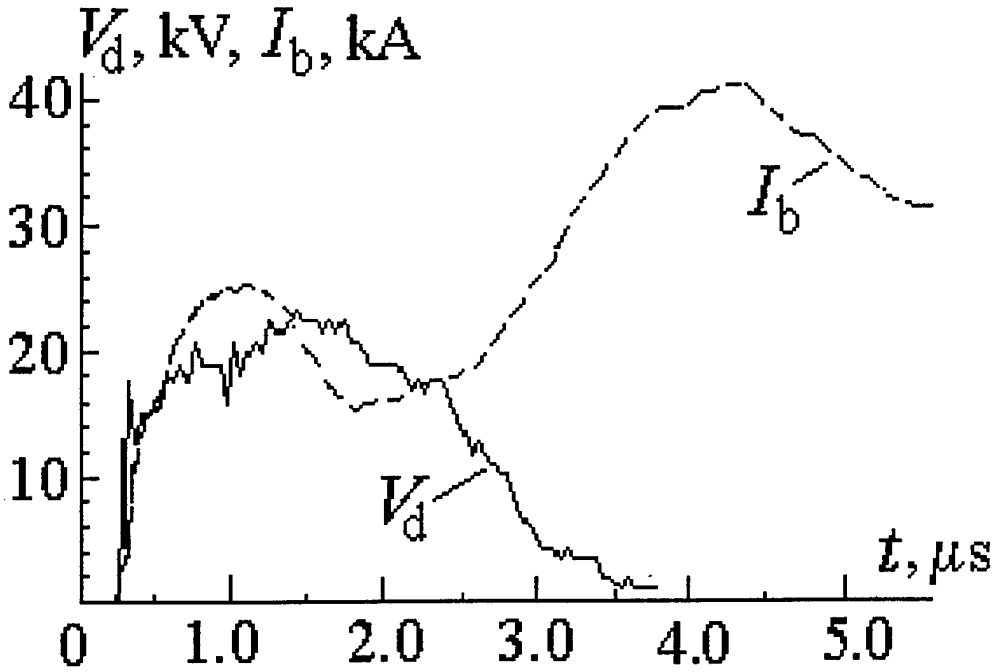

Fig. 3. Typical waveforms of diode voltage (V_d) and beam current (I_b)

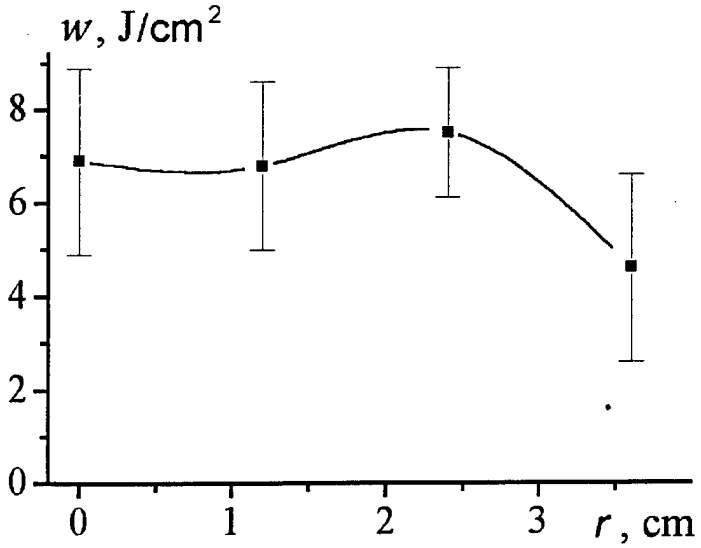

Fig. 4. Typical distribution of beam energy over the beam cross-section at H=1.5 kOe

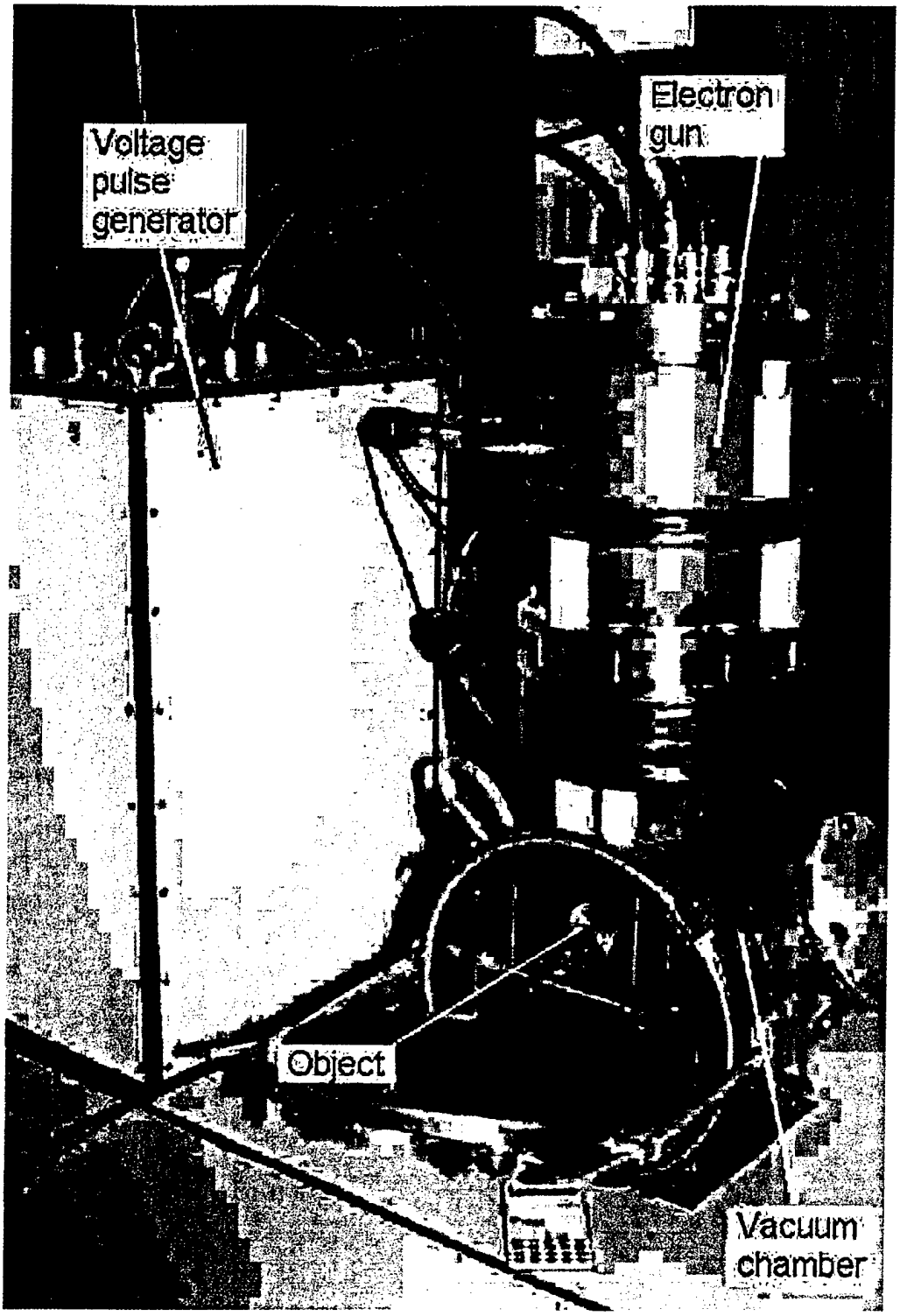

Fig. 5. Outer view of the e-beam setup

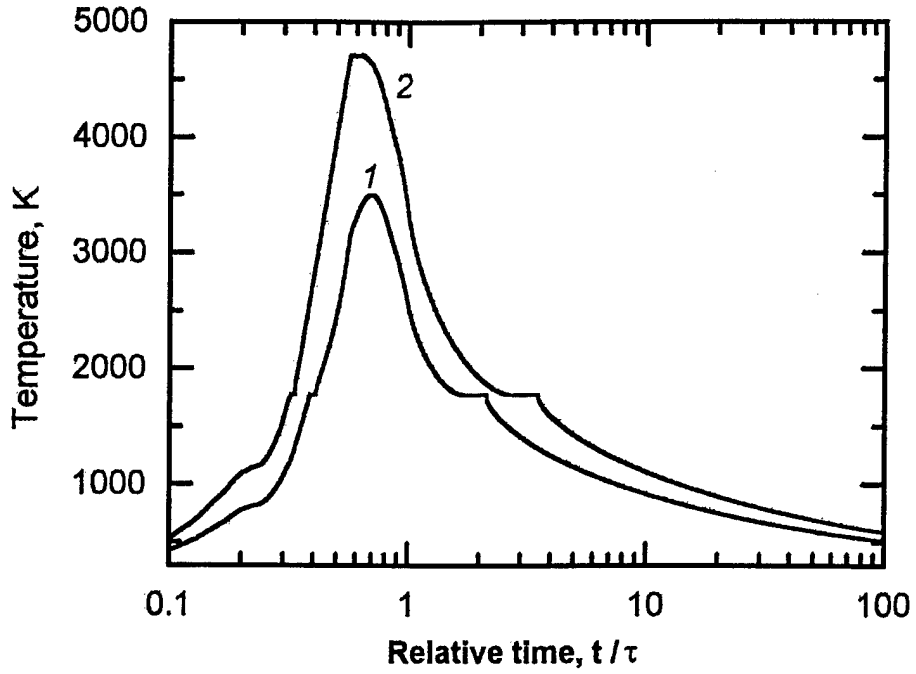

Fig. 6. Time dependence of the surface temperature for stainless steel irradiated at bean energy density of (*1*) 5 J/cm^2 and (*2*) 9 J/cm^2; τ is the beam pulse duration.

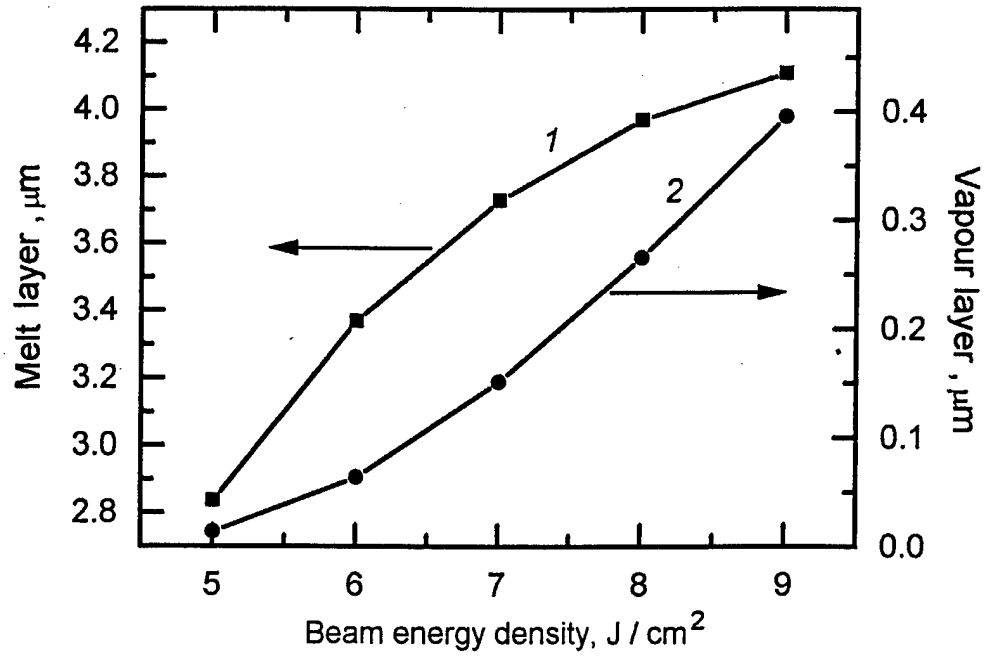

Fig. 7. Thickness of molten and evaporated layers vs e-beam energy density

3. STUDY OF POSSIBILITY OF INCREASING MICROWAVE OUTPUT POWER PULSE WIDTH IN A 3 GW BACKWARD WAVE OSCILLATOR

3.1. Experimental Setup

3.1.1. High-Current Electron Accelerator SINUS-7

The experiments on the BWO pulse lengthening were performed on the base of the electron accelerator facility SINUS-7. The high-current electron accelerator SINUS-7 (Fig. 8) is a direct action accelerator [18]. The high voltage pulse is produced in a coaxial pulse forming line (PFL) and delivered to the vacuum electron diode through a pulse transmitting line. Both the forming line and the transmitting line are oil-insulated. The high voltage switch that discharges the forming line onto the transmitting line is a Nitrogen spark gap switch pressurized up to 15 Atmospheres. The wave impedance of the PFL is 30 Ohm. To match the PFL with a vacuum electron diode having an 80 - 120 Ohm impedance, tapering of the transmission line is applied. The PFL is charged from a resonant Tesla transformer built in the line. The ferromagnetic code of the transformer is open and their magnetic conductors are coincident with the inner and outer conductors of the forming line. The transformer has a single-turn primary; and its conic secondary (item *2* in Fig. 8) is situated in the gap between the PFL conductors and counts 3840 turns. The pulse duration of the accelerator is determined by the double transit time of the PFL and equals 50 ns. The PFL charging voltage can reach 2.4 MV and can be controlled by adjusting the spark gap gas pressure. The wall-plug efficiency of the accelerator is about 60%. Thus, the maximum parameters of electron beam produced by the accelerator are 20 kA and 2 MV in the single-shot regime and 15 • • and 1.5 MV in the repetitive mode (at 100 pulses per second).

In 3-GW BWO experiments, a tubular electron beam was produced in a coaxial magnetically-insulated diode with a edge-type explosive-emission graphite cathode. The cathode diameter was 19 mm with the edge thickness of 0.5 mm. The magnetic field with the strength of up to 45 kOe was produced in a pulsed solenoid.

The schematic diagram of evacuation of the accelerator diode and electrodynamic system of the BWO is shown in Fig. 8. To eliminate oil vapor in the BWO volume, liquid nitrogen traps were utilized. One of the traps was inserted in the bypass between the roughing pump (two rotor oil pumps of • • • -5• type) and the evacuated volume that is the electron diode and the BWO electrodynamic system. The second - larger cross section - trap was placed in the main evacuation channel between the turbomolecular pump • • • -500 and the diode. The traps were intercepting the flow of oil molecules coming from the pumps into the vacuum diode. Thus, the vacuum system was providing oil-free evacuation to 10^{-4} Torr.

The microwave energy was radiated in air through a horn antenna with a half-opening angle of 6 deg. The microwave window made of 7-mm Lucite was 50 cm in diameter.

3.1.2. The Microwave Measurement System

The microwave pulse power measurement was utilizing a calibrated receiving antenna and a thermionic diode detector and was made by integration of power flow over the radiation pattern. The radiation wavelength was determined using a tunable narrow-band pass filter with half-amplitude bandwidth about 0.3%.

A thermionic diode detector provides monitoring of nanosecond microwave signals in the frequency range of 8 to 12 GHz. The detector was calibrated at 9.375 and 9.42 GHz. The schematic drawing of the thermionic diode detector is shown in Fig. 9. The detector diode is AC cathode heated 6D16D diode. However, instead of AC, stabilized DC power supply is used for the cathode heating. This provides more stable characteristic of the detector independent on fluctuations of power supply voltage. The matching load reduces the amplitude of the wave reflected from the diode. The dummy absorbs the wave passing through the diode. A low-pass filter is used to filter out microwaves and to transmit the detected signal to the oscilloscope. The detector V/W characteristic is given in the Appendix 1.

The resulting time resolution of the microwave measurement set up is of order of 1 ns. When measuring the BWO parameters, the distortion of detected nanosecond signal in the cable between the detectors and the oscilloscope was taken into account.

The receiving antenna (Fig. 10) is formed by 23×10 mm^2 waveguide section having an open end. To slow down the dependence of the antenna effective aperture on frequency absorbing plates are placed onto external wide waveguide sides. The standing wave coefficient of the antenna is 1.6 -1.9 in the frequency band from 9.1 up to 9.6 GHz. The measurement of dependencies of the antenna effective aperture on frequency is described in the Appendix 2.

Fig. 11 shows the schematic drawing of the band-pass filter. The band-pass filter consists of the input-output waveguide and the resonant waveguide. The resonant waveguide is plunged perpendicularly into the input-output waveguide and contains a shorting plunger moved with the use of precise screw so allowing the filter tuning. The waveguide section is 23×10 mm^2. The filter pass band width is 25-35 MGz in the frequency band from 9.1 up to 9.7 GHz. The calibration procedure for the band-pass filter is described in the Appendix 3.

For measurement of the energy in a microwave radiation pulse with power level of several gigawatts, we developed a calorimeter similar to that described in [19] but with greater cross section (about 250 mm). This allowed us to decrease the intensity of the microwave field on the surface of the absorbing element. The absorbing element was two nested glass tubes, the

gap between which was filled with water. The average diameters of the tubes were respectively 15 and 13 mm, the length of the tubes was 1200 mm, the mass of the absorbing layer of water was 47 g. A coil made of • • • -02 copper wire was wound on the inner tube. The resistance of the coil was about 140 Ohms. The change in the temperature of the water was measured from the change in resistance of the coil included in a bridge circuit. The sensitivity of the calorimeter was about 60 mV/J. The reflection coefficient of the circular waveguide TM_{01} wave relative to the calorimeter was not greater than 10%. For calibration of the calorimeter, a capacitor with known energy storage was discharged into the measuring coil, and then the change in its resistance was measured.

3.2. Study and Optimization of Parameters of Relativistic BWO with non LEHCEB-Treated Slow Wave Structure

An X-band relativistic BWO with microwave output towards the electron collector was explored (Fig. 12). The operating mode was TM_{01}. A beyond cutoff-neck (diameter 23 mm, length 40 mm) was providing the reflection of the operating wave at the cathode edge of the device. The SWS - a piece of circular corrugated wavequide - was consisting of separate rings. The SWS parameters were similar to that represented in [3] (corrugation amplitude 2.1 mm, average radius 1.5 cm, period 1.61 cm) but with increased number of periods (seven). The latter allowed for reducing the microwave oscillation build-up time in respect to electron beam pulse. The SWS and the cutoff-neck were made of stainless steel 12X18H10T. Unlike the experiment [3], electrochemical polishing of these components was made.

In the optimum generation regime (cathode voltage 1.2 - 1.3 MV, beam current 12 - 13 kA, magnetic field strength 35 kOe) the microwave pulse power was ranging 3 GW with 20% efficiency. The radiation wavelength measured by narrow-band filter was 3.18 cm. The radiation pattern was well corresponding to TM_{01} mode of circular waveguide.

Two different vacuum regimes were used in experiments. In the first one (below referred to as "oil vacuum") a turbomolecular pump was used. The second one (below referred to as "oil-free vacuum") additionally employed two liquid nitrogen traps as described above.

Under conditions of oil vacuum, the width of microwave pulses (measured at half amplitude) was about 16 ns with the standard deviation measured over ten pulses about 4%. The distinctive waveforms of the cathode voltage, electron beam current and microwave power are represented in Fig. 13. A significant (factor of two) increase in microwave pulse width comparing to [3] is due to electrochemical polishing of electrodynamic structure removing micro-spikes from its surface and therefore efficiently improving the SWS electric strength even in oil vacuum.

Oil-free evacuation of BWO to 10^{-4} Torr resulted in pulse lengthening up to 24 ns with 9.5% standard deviation. The corresponding distinctive waveforms of the cathode voltage, electron beam current and microwave power are represented in Fig. 14. Effect of SWS "training" in the intense RF field was observed in experiments. The width of the first pulse was not exceeding 16 ns. Then during several tens of pulses made without opening the vacuum system the pulse length was increasing up to the maximum value of 24 ns (Fig. 15).

In experiments, measurement of microwave pulse width as a function of generated power was made for invariable geometry of BWO electrodynamic system. Herewith the BWO output power was varied by different methods: changing the e-beam power, strength of guiding magnetic field, and vacuum diode impedance. Fig. 16 illustrates the dependencies of microwave pulse width on microwave pulse power for the above given SWS parameters under oil- and oil-free vacuum conditions. As is seen, the pulse width falls down as the microwave pulse power rises. The limitation of microwave pulse width in oil vacuum begins at a power level of about 1 GW, and in oil-free vacuum - about 2 GW.

At a microwave power of 2 GW, the maximum strength of RF electric field on the surface of SWS rings and the cutoff-neck estimates 1.5 MV/cm.

In those cases when microwave pulse shortening was occurring, visual erosion of metal surface was observed at the places of maximum RF electric field strength in SWS (namely, on the surface of the cutoff-neck and the first SWS period counting from the cutoff-neck, see Fig. 17). The size of craters was 10 – 50 μm. A similar erosion is found on metal explosive-emission cathodes. The prints on plastic targets (Fig. 18) indicated intense (~ 1 kA/cm^2) flow of electrons between SWS ripples. This high current density is peculiar to explosive electron emission.

These experimental results confirmed again that the presence of oil films, micro spikes and dielectric inclusions relieves the development of explosive emission on SWS surface and causes the microwave pulse shortening in the relativistic BWO.

3.3. Mechanism of Microwave Pulse Shortening

We assumed that the BWO pulse shortening occurs due to operating wave absorption by electrons emitted from the explosive-emission plasma on SWS surface. The generation process can terminate if the BWO critical current (starting current) becomes exceeding the current of the driving electron beam.

At the same time, nonlinearity of energy absorption by electrons with space charge limited current makes it incapable of terminating the generation. In fact, to increase the BWO starting current we should have a non-vanishing ratio between the wave power losses and the wave power flow at small field amplitude (the BWO efficiency tends to zero when approaching

the starting regime). The non-relativistic space charge limited current density for electrons is $j_{em} \propto E^{3/2}$ and the energy gained by electrons in the wave is $\varepsilon \propto E^2$ where • is the wave electric field strength. Thus, $P_{loss} \propto E^{5/2}$. Since the wave power $P_w \propto E^2$, have $P_{loss}/P_w \propto E^{3/2} \rightarrow 0$ at $P_w \rightarrow 0$. Thus, the non-relativistic space charge limited electron load can not effect the BWO starting current. Besides, account the presence of high-current driving electron beam with the electrostatic potential of $\sim 10^5$ V with respect to waveguide wall. If the microwave power falls below a definite level, the RF electric field drawing the electrons from the slow wave structure surface is totally compensated by the beam static field that makes the electron emission impossible.

However, the termination of generation can be explained in terms of electron absorption of the wave accounting the fact that positively charged ions are extracted from the plasma in appropriate phases of RF oscillation. The cyclotron radius for ions far exceeds that for electrons and can be comparable with the transverse size of SWS. Therefore, at initial moments of time, ions move towards the SWS axis tending to compensate the space charge of the driving electron beam. For single-charged ions, the density to compensate a 10-kA electron beam is $\sim 10^{11}$ cm^{-3}. The time of compensation ranges units of nanoseconds for light ions (e.g. protons, carbon ions) as follows from estimations and numerical experiment.

Due to space charge compensation, the electric field drawing the electrons from SWS surface is reaching full amplitude of the wave field • $_0$. This speeds up the excitation of explosive emission that possibly develops in avalanche manner, accounting the fact of separate emission center current growing in time as $t^{3/2}$.

Simultaneously, accumulation of ions in the space between SWS ripples occurs. Electrons emitted from the plasma move along magnetic field lines and their space charge additionally drives the accumulation of ions. In a conventional (non-oversized) BWO with the electric field strength of 10^6 V/cm electrons emitted from one ripple can reach another one during one RF period. Since the electron current is space charge limited, it creates a quasi-static field of average value in the order of • $_0$. In this field, ions move in accelerating manner and fill the gap in few nanoseconds (in absence of electron current the ion motion would be a cyclic drift so that the process would take hundreds of nanoseconds).

As a result, quasi-neutral plasma is formed in the gap between ripples. The space charges of ions and electrons are compensated in average during RF period. The concentration of plasma grows in time and so does the electron bombardment power. The following excess of the BWO starting current above the current of the driving electron beam results in the decay of microwave generation taking few nanoseconds.

The full-scale time-dependent numerical experiments employing the KARAT code [20] indicated that the combined electron-ion emission from SWS and beyond cutoff-neck could significantly decrease the BWO microwave power up to total suppression of generation.

Fig. 19 represents the configuration of electron beam and ion cloud (protons) in the relativistic BWO simulated using KARAT code for three different places of explosive emission (the beyond cutoff-neck, middle of the SWS, and its output edge). The maximum suppression of the generation was observed in the first case (Fig. 20). The typical concentration of explosive-emission ions and electrons in the proximity of emitting regions was ranging $5*10^{12}$ cm^{-3}.

Thus, termination of microwave pulse in a relativistic BWO may be caused by explosive emission on the SWS surface and absorption of the operating wave by electrons flowing between the ripples. The intensity of absorption is strongly increased due to ion compensation of electron charge. The width of microwave pulse is limited by the period of explosive emission development and the time of accumulation of ions in the SWS volume.

3.4. Study of Relativistic BWO with LEHCEB-Treated Slow Wave Structure

The BWO electrodynamic system parameters and the generation regime were the same as listed in 3.2. At a diode voltage of 1.2 - 1.3 MV, electron beam current of 12 - 13 kA, and magnetic field strength of 35 kOe the microwave power ranged 3 GW at a wavelength of 3.18 cm.

The BWO and the vacuum diode were evacuated to 10^{-4} Torr or better. Liquid nitrogen traps were installed in the evacuation channels (as described above) providing oil-free vacuum conditions.

In these experiments, as well as in that described in 3.2, the effect of BWO SWS "training" by intense microwave field was observed. Note that the duration of first microwave pulse was to some extent larger than mentioned in 3.2 and ranged 20 ns. Then during 15 - 20 pulses made without opening the vacuum system the pulse width was increasing reaching the maximum of 29 ns (Fig. 21). The mean-square deviation of pulse width measured over 10 pulses was about 5%.

The typical waveforms of diode voltage, beam current and microwave power pulses are represented on Fig. 21. As is seen, the fall of microwave pulse is coincident with the fall of the electron beam pulse so that we can not note a pulse shortening at such electron beam pulse duration.

The microwave pulse energy measured by means of a calorimeter (see 3.1) was about 80 J.

The microwave pulse width did not change at lower electron beam powers as well as at different magnetic field strength (Fig. 16). A gentle increase of microwave pulse width observed at 1.5 GW microwave power was due to shorter build-up time of BWO oscillation.

During about 200 pulses made without opening the vacuum system, no notable changes in the microwave pulse duration was observed.

In the region of maximum strength of RF electric field (beyond cutoff-neck and the first SWS ring) erosion spots were found similar to that represented in Fig. 17. However, the number density of craters in these spots was 2 - 3 times less than in the case of non-treated SWS.

Filling the SWS with air was forming an oxide film on its surface. The width of microwave pulses made after this procedure was not exceeding 24 ns.

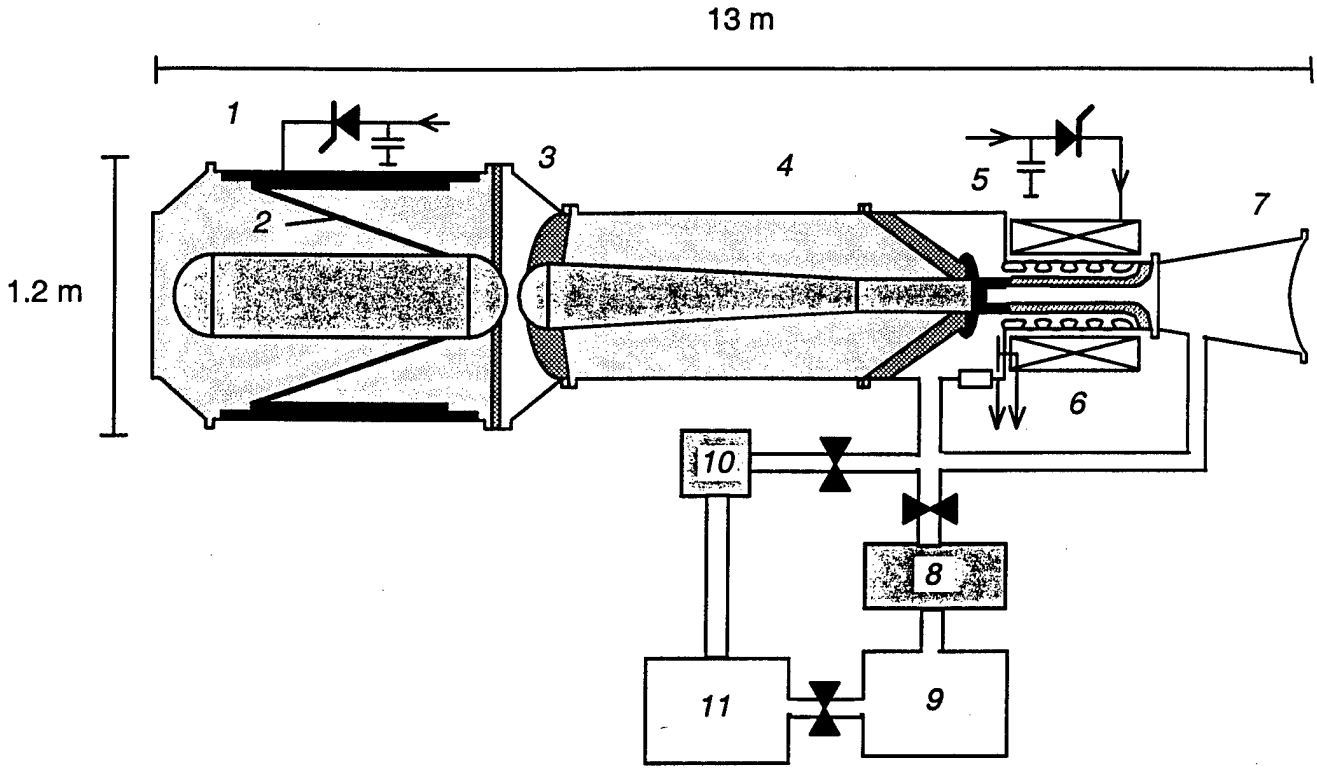

Fig. 8. Experimental setup SINUS-7.

1 - Pulse forming line with built-in Tesla transformer
2 - Secondary coil of the Tesla transformer (newly replaced)
3 - Pressurized high-voltage gas gap switch
4 - Pulse transmitting line
5 - Vacuum Electron diode
6 - BWO slow wave structure and magnetic field coil
7 - Vacuum window for microwave output
8, 10 - cryogenic vacuum traps (newly installed)
9 - turbo molecular pump
11 - roughing pump

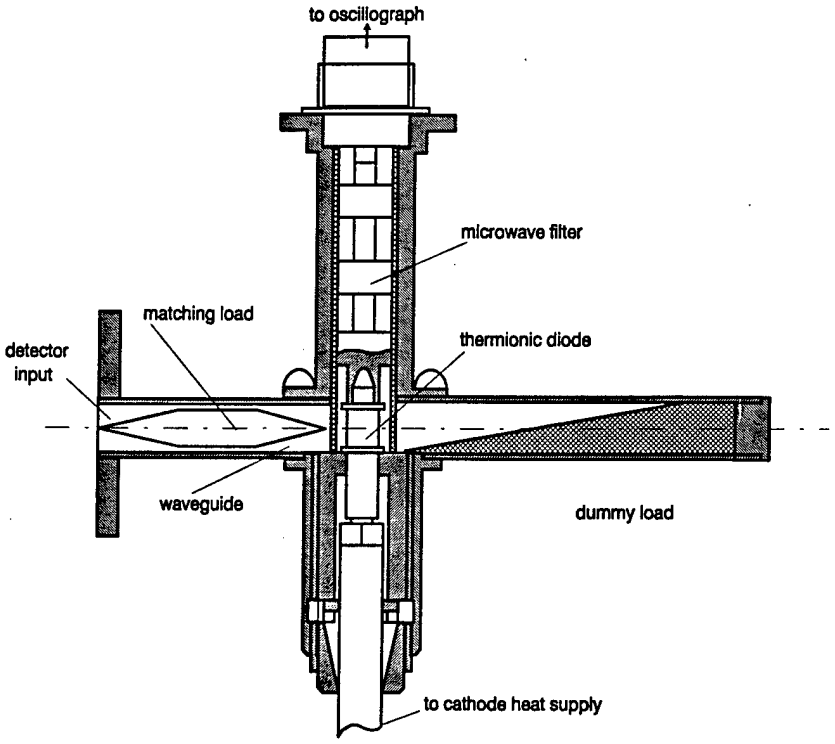

Fig. 9. Schematic drawing of the thermionic diode detector

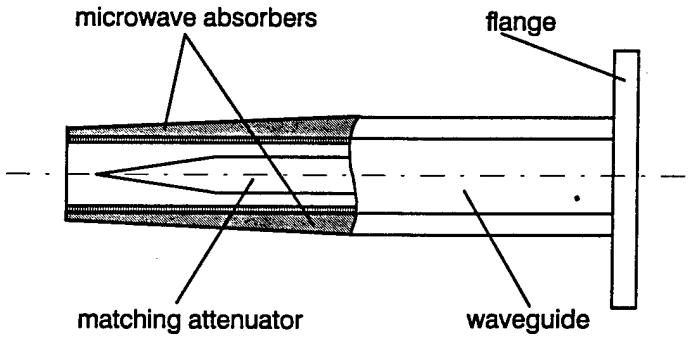

Fig. 10. Schematic drawing of the receiving antenna

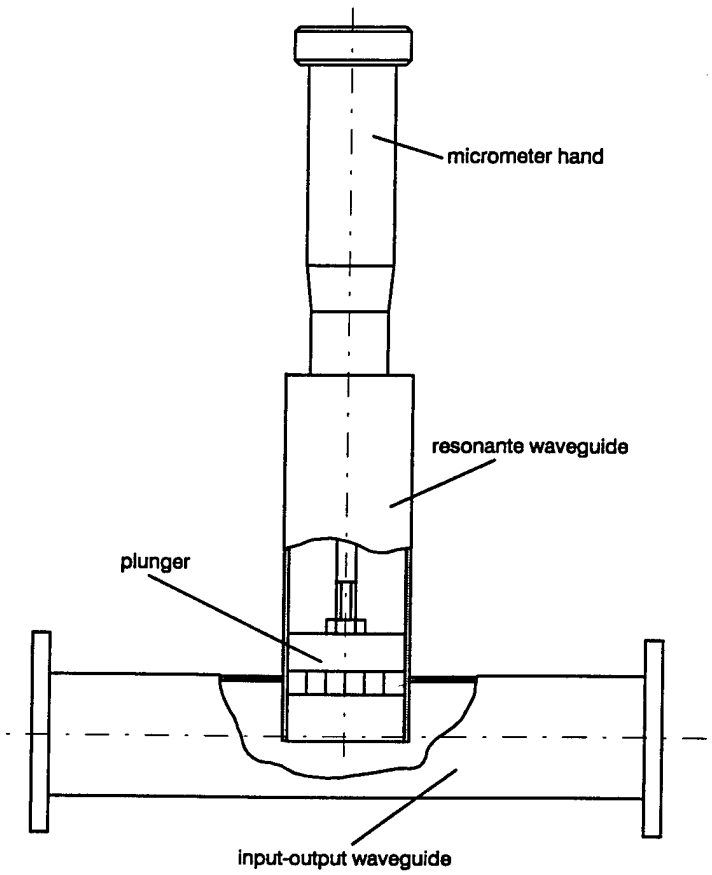

Fig. 11. Schematic drawing of the band-pass filter

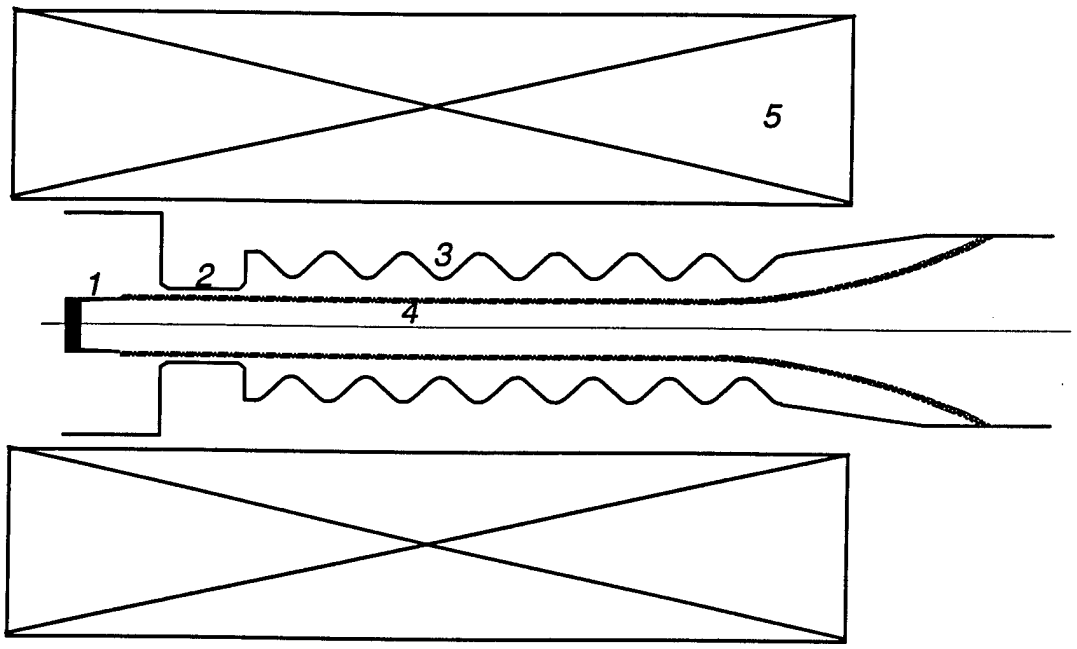

Fig. 12. Geometry of the relativistic BWO. *1* - tubular explosive-emission cathode, *2* - beyond cutoff-neck, *3* - SWS, *4* - electron beam, *5* - magnetic coil.

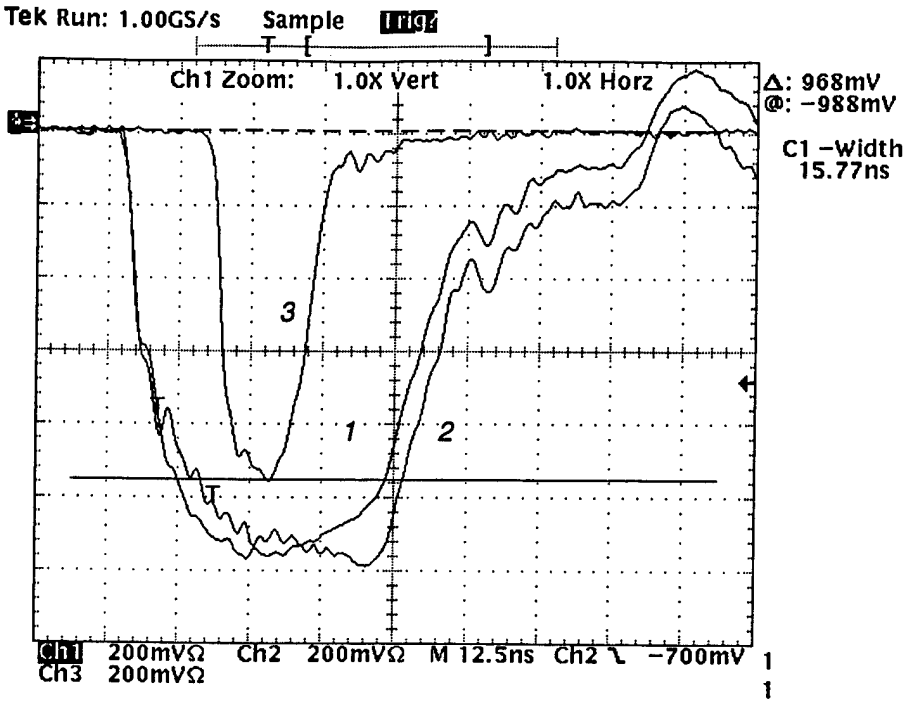

Fig. 13. Waveforms of (1) diode voltage, (2) e-beam current, and (3) microwave detector signals. Oil vacuum, non-LEHCEB-treated SWS.

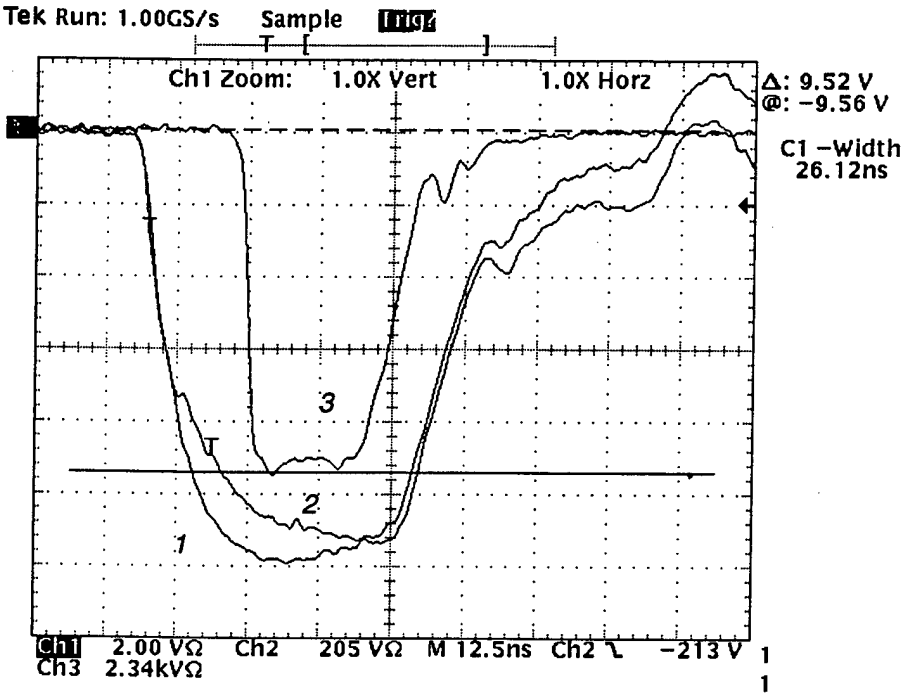

Fig. 14. Waveforms of (1) diode voltage, (2) e-beam current, and (3) microwave detector signals. Oil-free vacuum, non-LEHCEB-treated SWS.

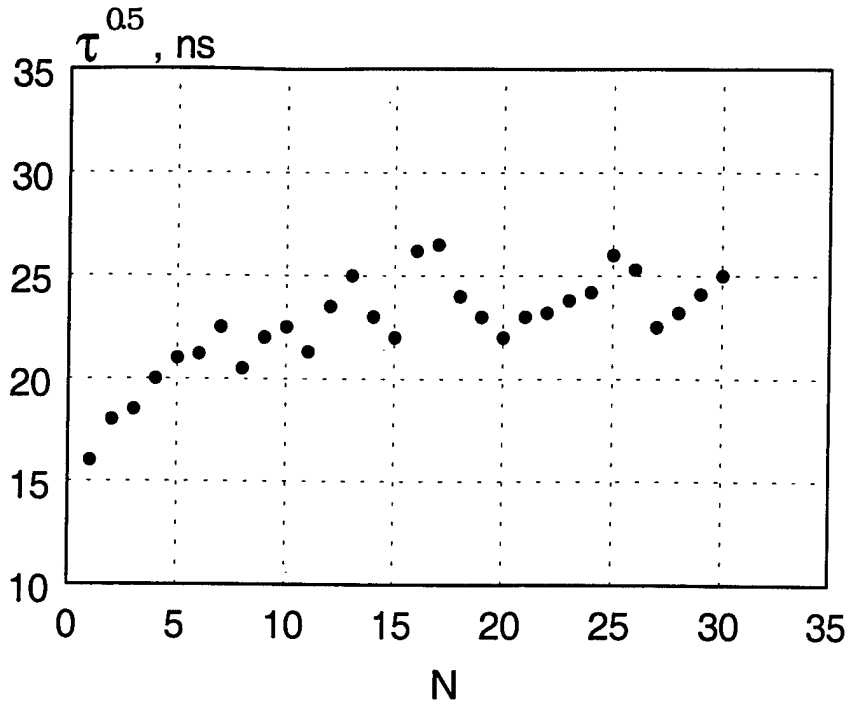

Fig. 15. Dependence of microwave pulse width on the number of pulses (oil-free vacuum, non-LEHCEB-treated SWS).

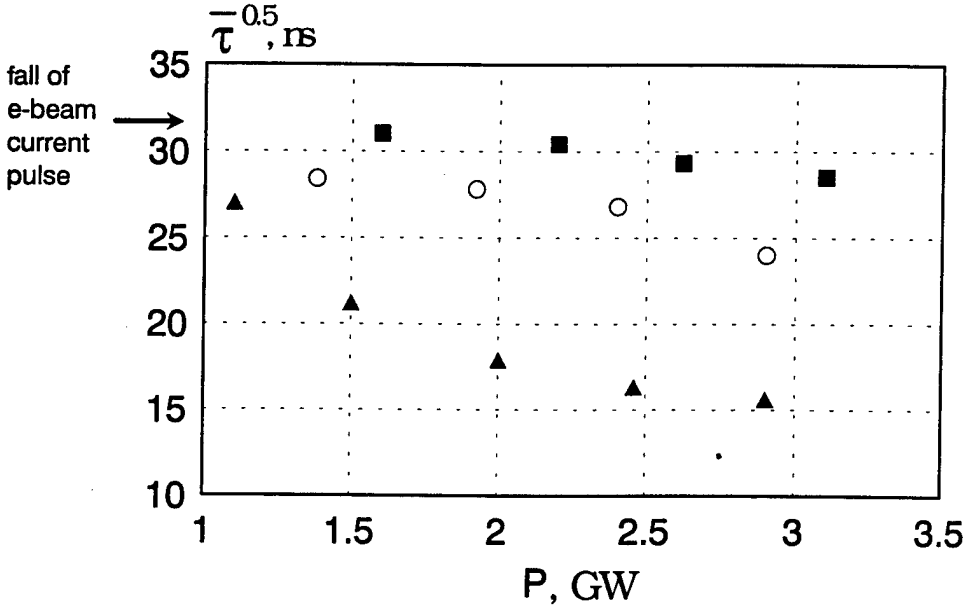

Fig. 16. Microwave pulse width vs power.

Triangles - oil vacuum, electrochemically polished SWS

Circles - oil-free vacuum, electrochemically polished SWS

Squares - oil-free vacuum, LEHCEB-treated SWS

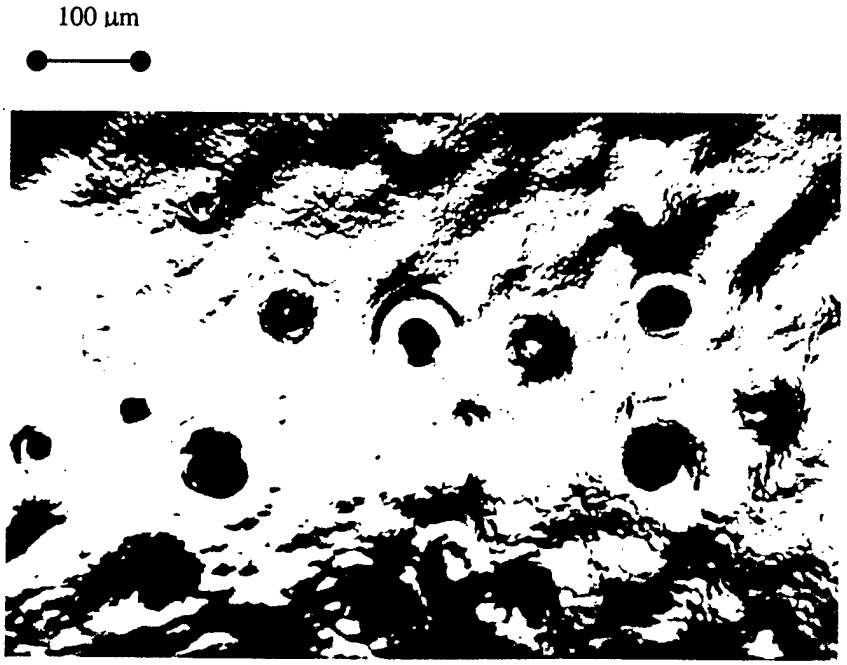

Fig. 17. Microcraters of erosion on the surface of the BWO beyond cutoff-neck and first SWS ring

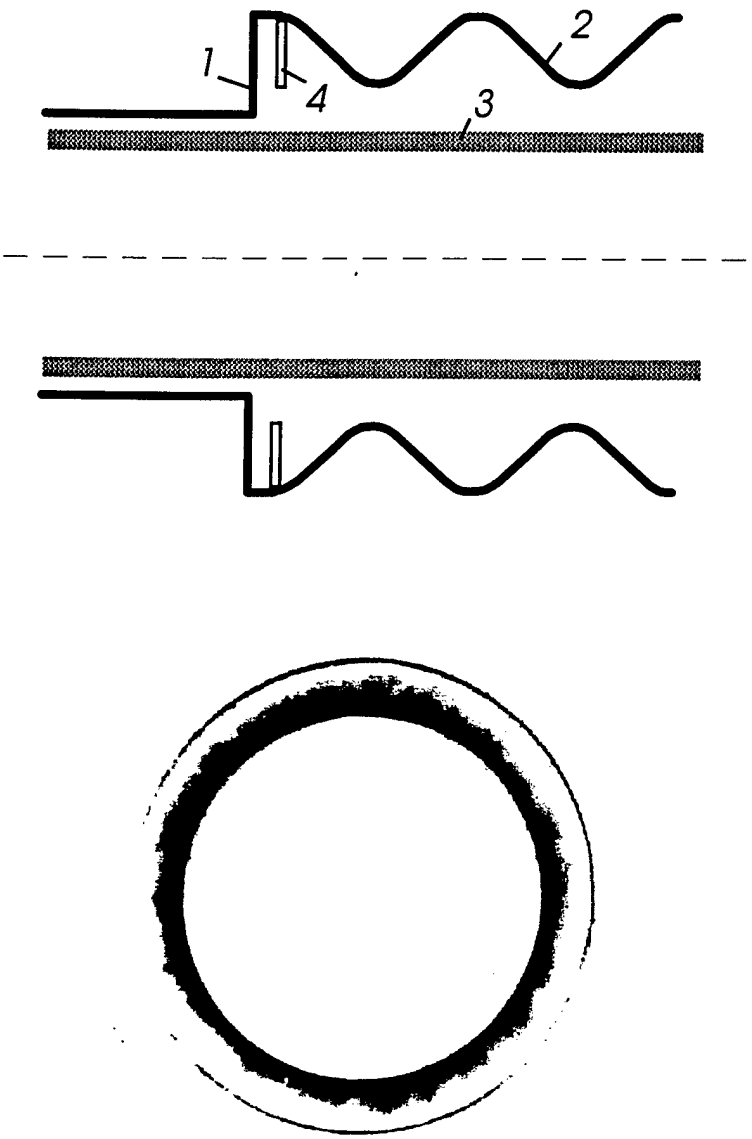

Fig. 18. Taking print of electron current flowing between SWS ripples.

1 – beyond cutoff-neck, *2* – SWS, *3* – e-beam, *4* – plastic target.

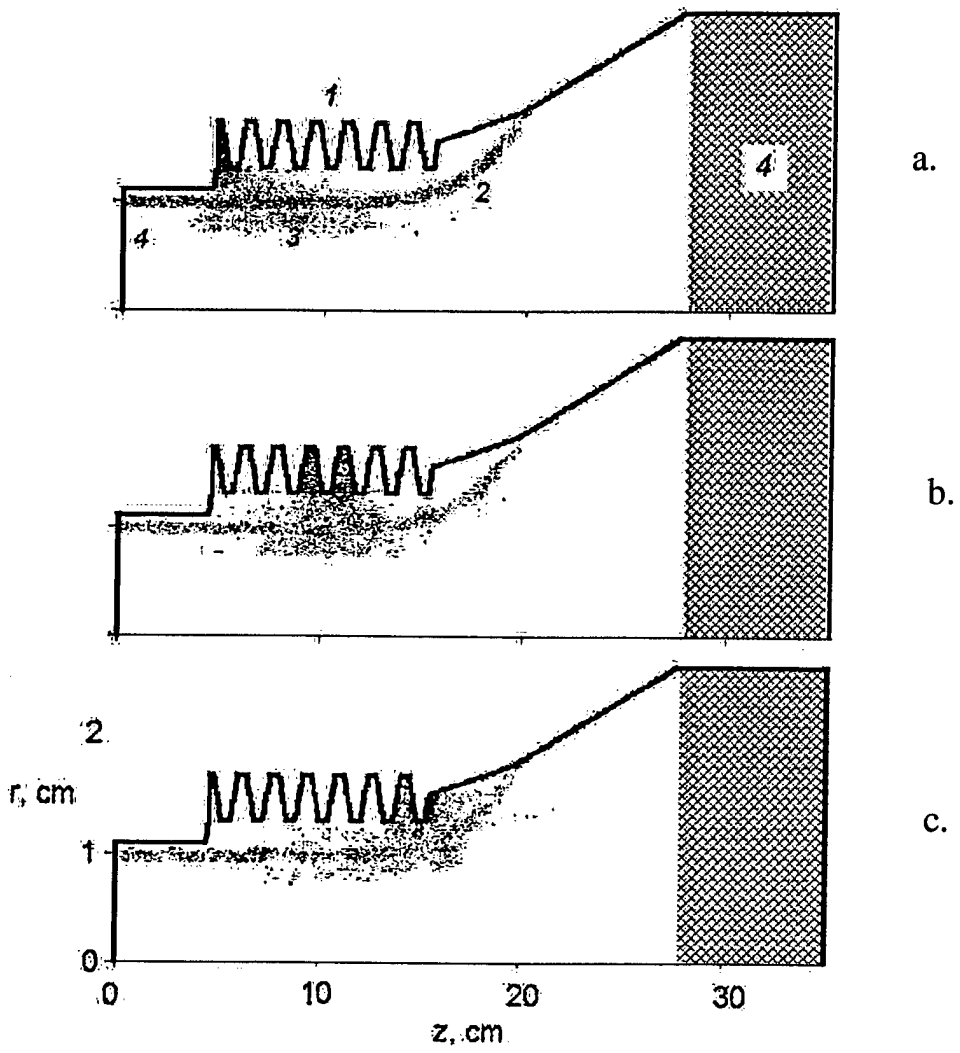

Fig. 19. Simulated configuration of BWO with electron and ion emission from SWS surface (KARAT code). *1*- SWS, *2* - driving REB, *3* - ion cloud (protons), *4* - beyond cutoff-neck, *5* - microwave absorber.

a - emission from cutoff-neck

b - emission in the middle of SWS

c - emission at the output of SWS

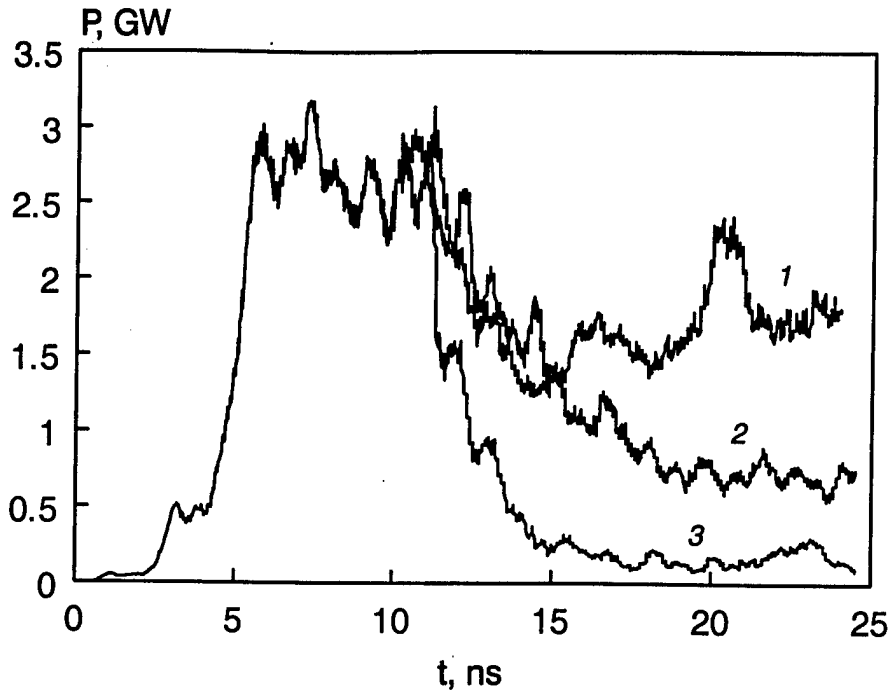

Fig. 20. Simulated waveforms of microwave power from the BWO with electron and ion emission on SWS surface (emission starting at t=10 ns).

1 - emission at the output of SWS

2 - emission in the middle of SWS

3 - emission from the cutoff-neck

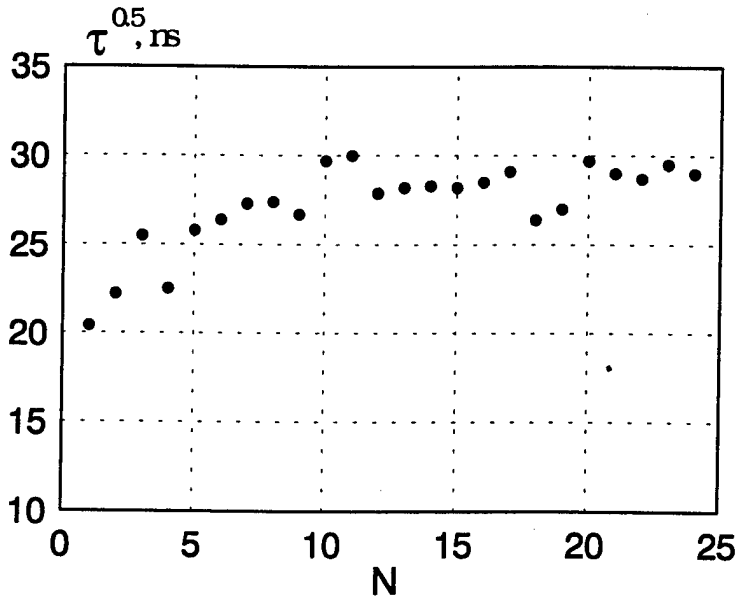

Fig. 21. Dependence of microwave pulse width on the number of pulses (oil-free vacuum, LEHCEB-treated SWS).

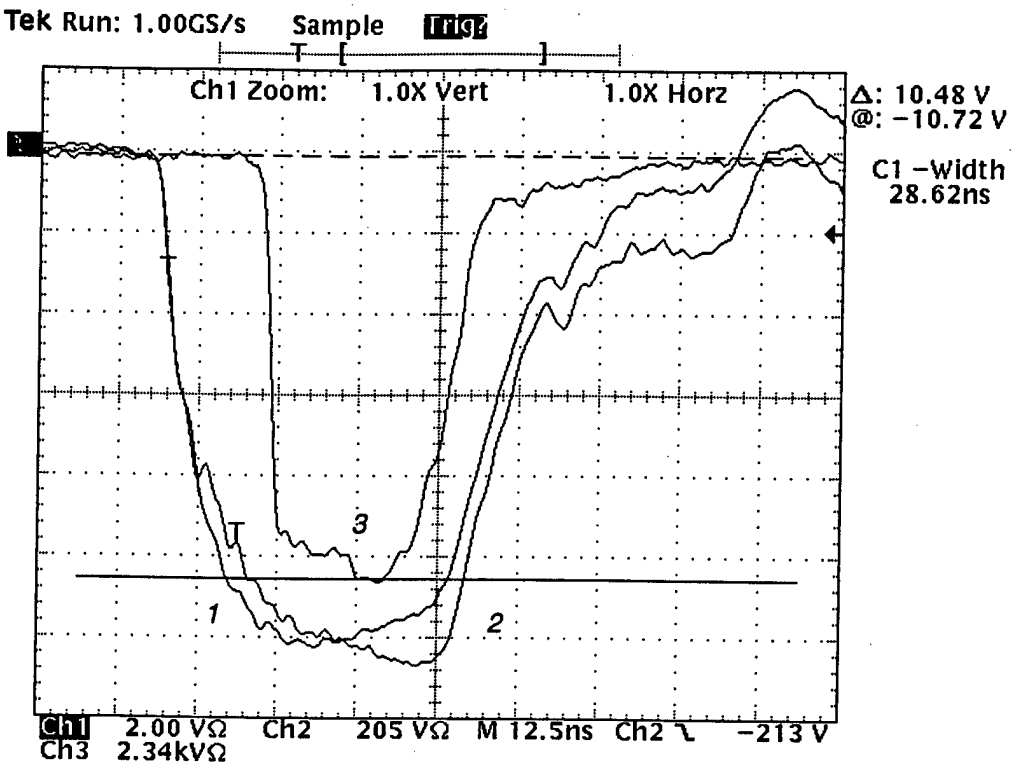

Fig. 22. Waveforms of (1) diode voltage, (2) e-beam current, and (3) microwave detector signals. Oil-free vacuum, LEHCEB-treated SWS.

4. CONCLUSIONS

The pulse shortening occurring in the relativistic BWO at gigawatt power level is escorted by appearance of explosive-emission plasma on the surface of the slow wave structure. The reason of microwave pulse termination is the increase of the BWO starting current due to partial absorption of the electromagnetic wave by electrons emitted from the plasma. The intensity of absorption is strongly increased by ions emitted from the plasma due to compensation of electron space charge. Thus, the width of microwave pulse limited by this mechanism is determined by the time of excitation of the explosive emission on the slow wave structure surface and the time of accumulation of ions in its volume.

The treatment of BWO slow-wave structure surface by low-energy high-current electron beam allowed for microwave pulse lengthening up to 30 ns at 3-GW power level. Herewith, the fall of the microwave power pulse was coincident with the fall of the driving electron beam pulse.

The presence of oil vapors in the slow-wave structure decreases the microwave pulse width for almost two times.

Formulate some recommendations on possible further studies:

1. Using the electron accelerator SINUS-7 at IHCE, perform experiments to determine the lifetime for the 3-GW BWO with LEHCEB-treated slow wave structure (make up to 10^4 pulses).
2. Using a long-pulse electron accelerator (several hundreds of nanoseconds), study the behavior of BWO with LEHCEB-treated slow wave structure and determine the limit for pulse lengthening. An electron accelerator with appropriate parameters (PI-110) is available at the University of New Mexico, Albuquerque, USA (Pulsed Power and Plasma Science Lab, Prof. Edl Schamiloglu).

5. REFERENCES

1. Zaitsev N. I., et al. // Lett. J. Tech. Phys. (Sov.). 1981. V. 7. No. 14. P. 879.
2. El'chaninov A. S., et al. // Lett. J. Tech. Phys. (Sov.). 1981. V. 7. No. 19. P. 1168-1171.
3. Gunin A. V., et al. // Russian Physics Journal. 1996. V. 39. No. 12. PP. 1229-1232.
4. Aleksandrov A. F., et al. // Abstr. 4th Symp. High-Current Electronics. - Novosibirsk, 1982. PP. 168-171.
5. Aleksandrov A. F., et al. // Relativistic High Frequency Electronics. Issue 3. - Gorky, 1983. PP. 219-240.
6. Mesyats G. A. // Proc. Course and Workshop on HPM Generation and Applications / Villa Monastera - Varenna, Italy. 1991. PP. 345-362.
7. Benford J., Benford G. // IEEE trans. Plasma Sci. 1997. V. 25. No. 2 PP. 311-317.
8. Kovalev N. F., et al. /// IEEE Trans. Plasma Sci. 1998. V. 26. No 3. PP. 246-251.
9. Loza O. T., Strelkov P. S. // Dig. Tech. Papers, Int. Workshop on HPM generation and Pulse Shortening. Edinburg, UK, 1997. PP. 103-108.
10. Latham R.V. High Voltage Vacuum Insulation. London: Academic Press. 1981.
11. Mesyats G. A. and Proskurovsky D. I. Pulsed Electrical Discharge in Vacuum/ Berlin: Springer-Verlag, 1989.
12. Batrakov A. V., et al. // IEEE Trans. Diel. and Electr. Insul. 1995. V. 2. No. 2. PP. 237-242.
13. Batrakov A. V., et al. // IEEE Trans. Diel. and Electr. Insul. 1997. V. 4. No. 6. PP. 857-862.
14. Batrakov A. V., et al. // Proc. of the 11th IEEE Int. Pulsed Power Conf., Baltimore, USA, 1997. PP. 519-524.
15. Ozur G. E. and Proskurovsky D. I. // Proc. of the 7th Int. Symp. on Discharges and Electr. Insul. in Vacuum (ISDEIV-90), 1990, Santa Fe, USA. PP. 665-670.
16. Nazarov D. S., et al. // Proc. of the 11th IEEE Int. Pulsed Power Conf., Baltimore, USA, 1997. PP. 1335-1340.
17. Proskurovsky D. I., et al. // I. Vac. Sci. and Tecnol. A, 16(4), Jul/Aug, 1998. PP. 2480-2488.
18. Korovin S. D. and Rostov V.V. // Russian Phys. J.1996. V. 39. No. 12. PP. 98-109.
19. Klimov A. I. // Russian Phys. J. 1996. V. 39. No. 12. PP. 1177-1185.
20. Tarakanov V. P. User's Manual for Code KARAT. - Springfield: BRA, 1992.

APPENDIX 1. CALIBRATION OF THE MICROWAVE DETECTOR

The thermionic diode detector calibration was made at the frequencies f = 9.375 and 9.42 GHz. The scheme of calibration of the detector and its V/W characteristic are shown in Fig. A1.1 and Fig. A1.2 respectively.

A 0.8-μs pulsed microwave power up to several tens of kilowatts was supplied from a high power frequency tunable magnetron and varied by an attenuator. The average power was measured with the use of the power meter M3-22A and a coupler. The calibrated detector signal $U(t)$ was monitored by C8-14 oscilloscope. To filter out the bias voltage, an RC-filter-divider with 4.6 attenuation coefficient was used. The current value of power $P(t)$, the average power P_{av} measured with the use of power meter, and the pulse repetition frequency $f_{rep} \approx 46$ Hz are related as $P_{av} = f_{rep} E_{sing} / k_c$ where $E_{sing} = \int_0^{\tau} P(t)dt$ is the single microwave pulse energy, τ is the full pulse duration.

To measure the waveform of microwave pulse $P(t)$ a special detector operating in quadratic mode ($U(t) \sim P(t)$) was used preliminary. This detector was connected to the coupler instead of the power meter to provide low level of pulse power. This allows calculation of the wave form coefficient k_{wf}:

$$k_{wf} = \frac{1}{\tau P_0}\int_0^{\tau} P(t)dt = \frac{1}{\tau U_0}\int_0^{\tau} U(t)dt$$

where P_0 is the amplitude microwave power at the input of the detector. Thus, the amplitude of microwave power P_0 which corresponds to a definite signal amplitude U_0 can be determined as

$$P_0 = \frac{P_{av} k_c}{k_{wf} f_{rep} \tau}$$

This relation allows to determine P_0 for measured values of P_{av} and U_0.

The total error Δ of the detector calibration was determined by the systematic errors θ_i of k_{wf} (±5%), k_c (±7%), P_{av} (±15%), deviation coefficient of the oscilloscope (±4%), oscilloscope scanning (±5%) and the total casual error of single calibration $\sigma(x)$ = ±8,6%.
The total error of calibration was calculated according to the formula

$$\Delta = \sqrt{\sigma^2(\bar{x}) + \theta_{\Sigma}^2} \quad , \text{where } \theta_{\Sigma} = 1{,}1\sqrt{\sum_{i=1}^{M} \theta_i^2}.$$

and was equal to Δ = ±22%.

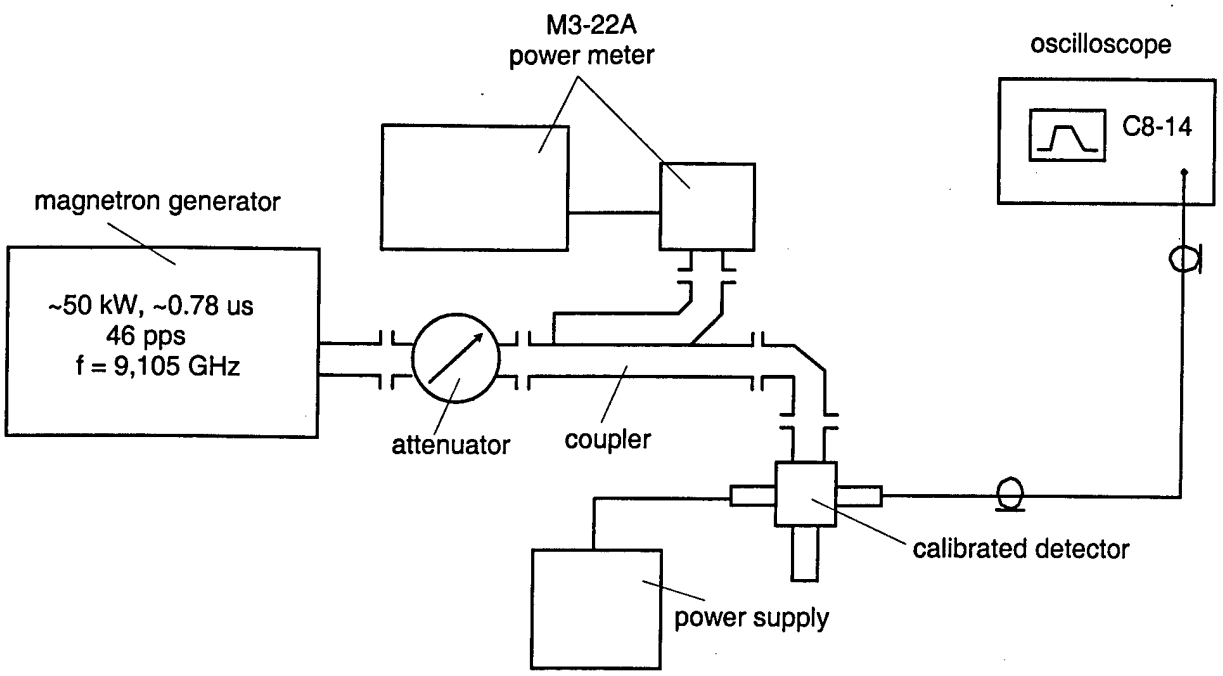

Fig. A1.1. Scheme of thermionic diode microwave detector calibration

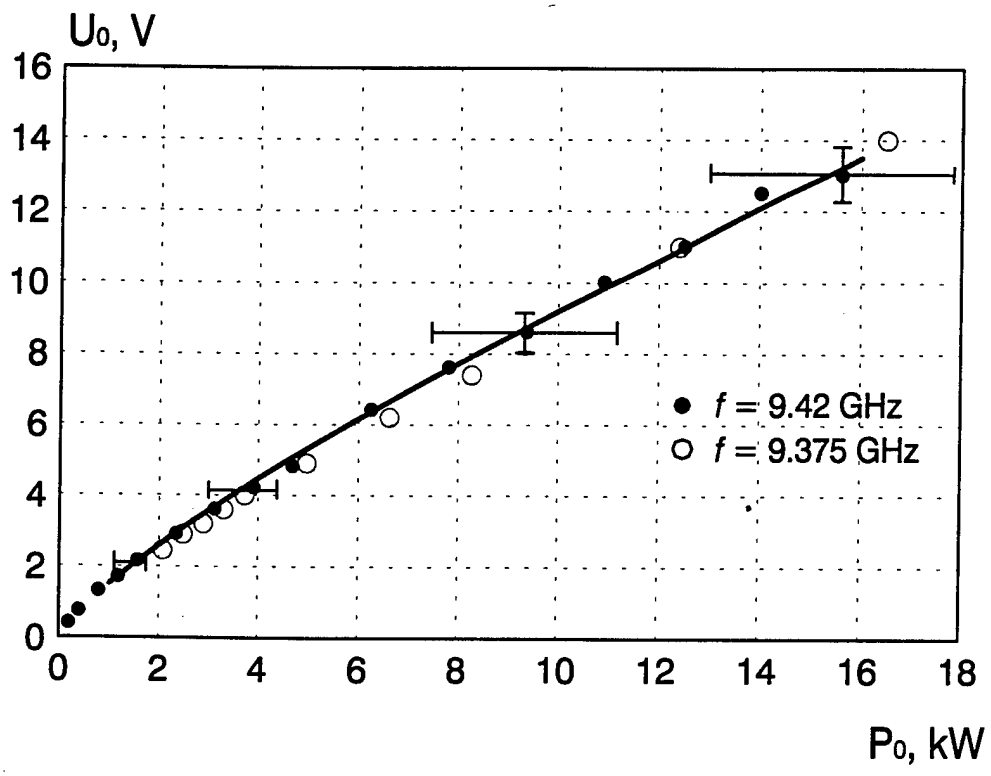

Fig. A1.2. V/W characteristic of the thermionic diode detector

APPENDIX 2. MEASUREMENT OF WAVEGUIDE ANTENNA EFFECTIVE APERTURE

The waveguide antenna was calibrated according to scheme shown in Fig. A2.1. The results are presented in Fig. A2.2. To calibrate the waveguide antenna the radiolocation equation was used:

$$\frac{P_R}{P_T} = \frac{S_{ef.T} S_{ef.R}}{\lambda^2 r^2} \qquad (1)$$

where $S_{ef.T}$ and $S_{ef.R}$ are effective absorbing apertures of transmitting and receiving antennas respectively, P_T and P_R are the transmitted and received microwave powers, λ is wavelength, r - distance between phase centers of the antennas. The difference in distances between phase centers and apertures of antennas was actually very small so the value r was supposed to be equal to the distance between apertures of the antennas.

At the first stage, effective absorbing apertures $S_{ef.T} = S_{ef.R} = S_{ef}$ of two identical rectangular horn antennas were measured. In this case, the relation (1) may be represented as

$$S_{ef} = \lambda r \sqrt{\frac{P_R}{P_T}}.$$

Then the waveguide antenna was installed instead of receiving horn antenna and the effective aperture was measured from the changes of the ratio P_R/P_T.

To measure the P_R/P_T ratio, a panoramic attenuation meter P2-61 was used according to the scheme shown in Fig.2.1. To check the P2-61 attenuation data, the precise attenuator D3-33A was used. To measure λ, the precise frequency meter • 3-66 was used. The error of waveguide antenna effective aperture measurement was not more ±20%, mainly due to error of P_R/P_T measurement (±7%) and the presence of certain level of standing wave (±15%) and cross-polarization (±5%). The error of λ measurement was ±0.1%. The error of r - measurement was ±1%.

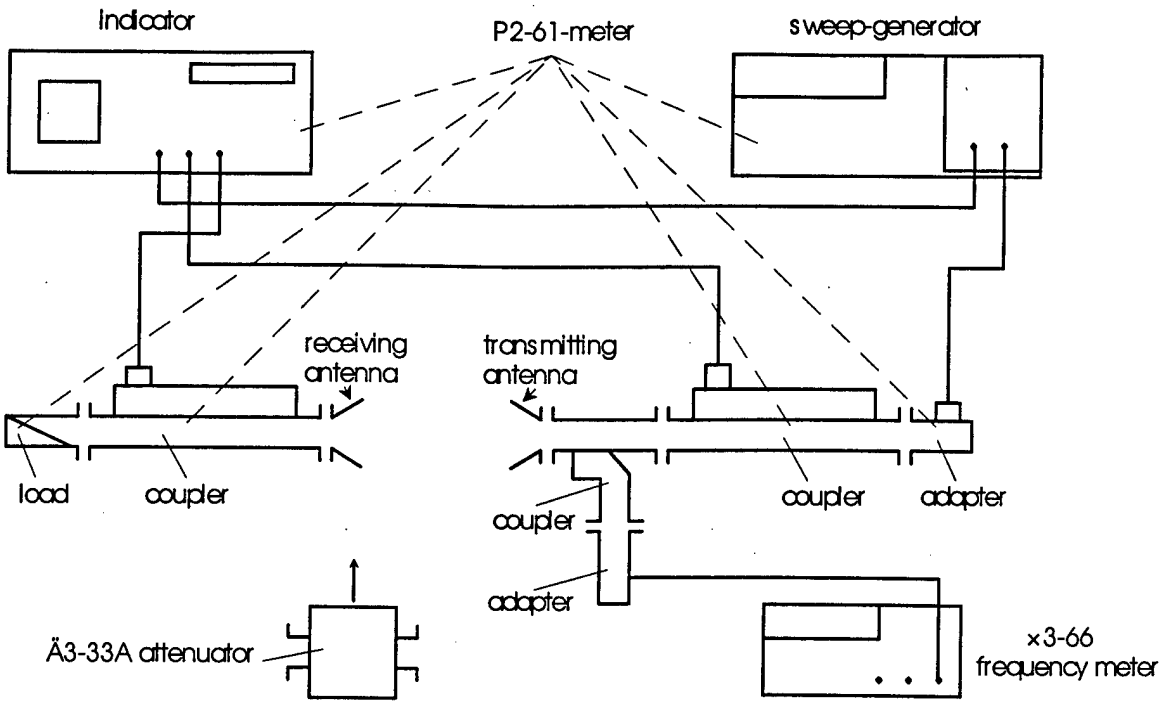

Fig. A2.1. Scheme of waveguide antenna effective absorbing aperture measurement

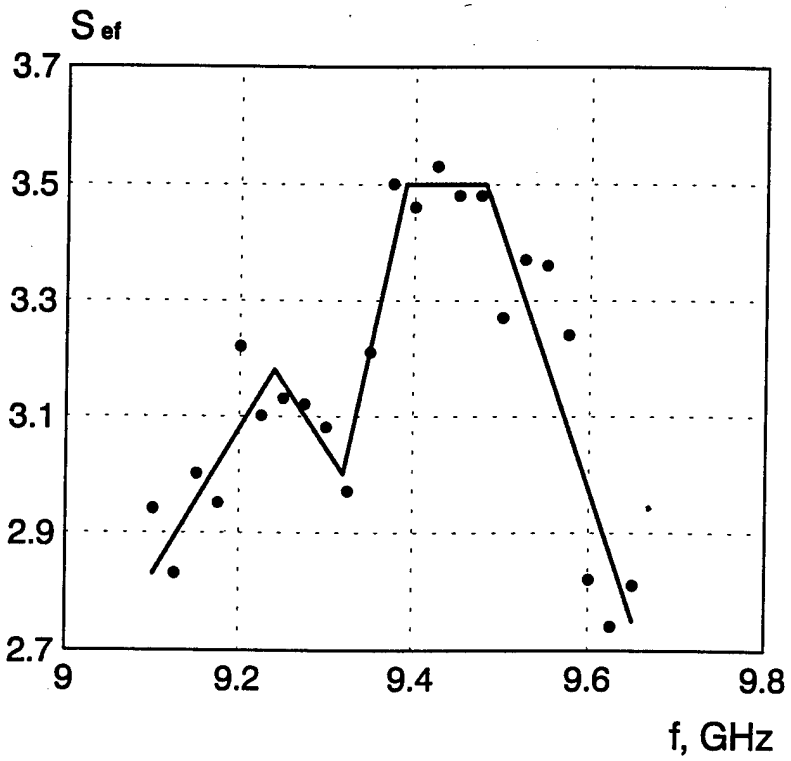

Fig. A2.2. Effective aperture of the waveguide antenna vs frequency

APPENDIX 3. CALIBRATION OF THE BAND-PASS FILTER

The band-pass filter was calibrated according to scheme shown in Fig. A3.1. The results are presented in Fig. A3.2.

To measure the characteristic of the filter, the panoramic attenuation meter P2-61 was used. Precise attenuator D3-33A allowed for more exact measurement of attenuation of the filter. Precise frequency meter • 3-66 was used for more accurate measurement the filter resonant frequency and band-pass width.

The error of frequency measurement was ±0.2. The error of attenuation measurement was ±6%.

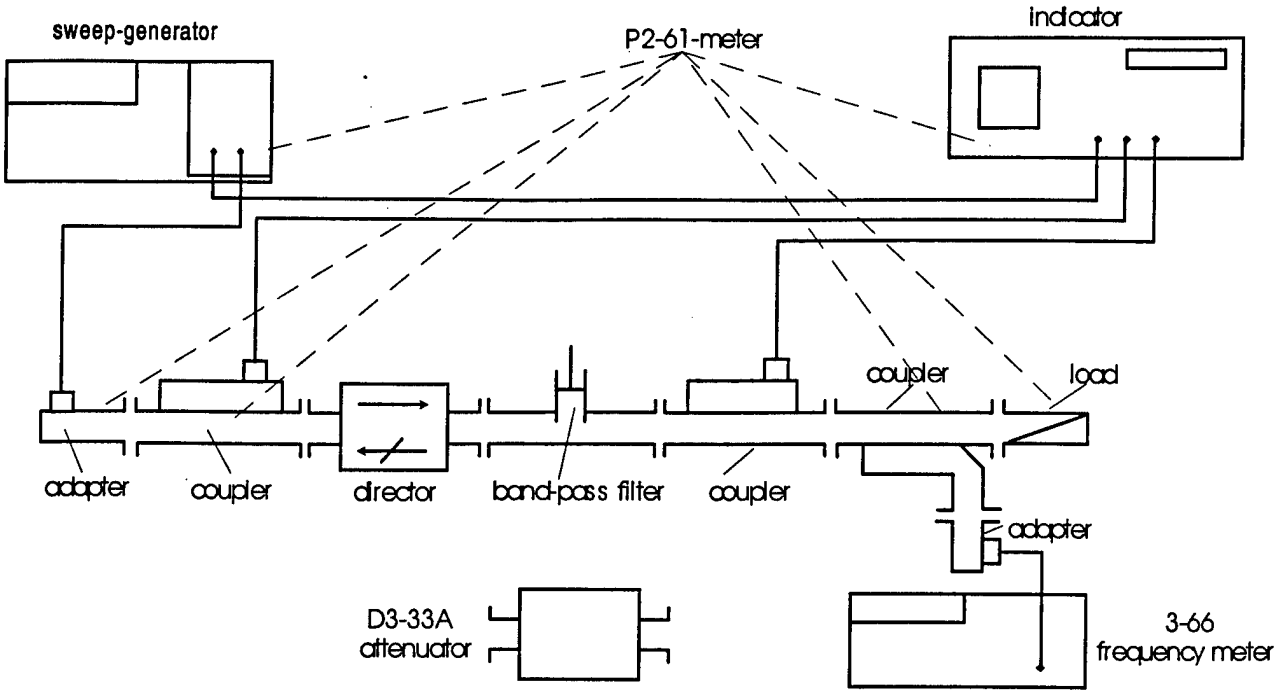

Fig. A3.1. Scheme of band-pass filter calibration

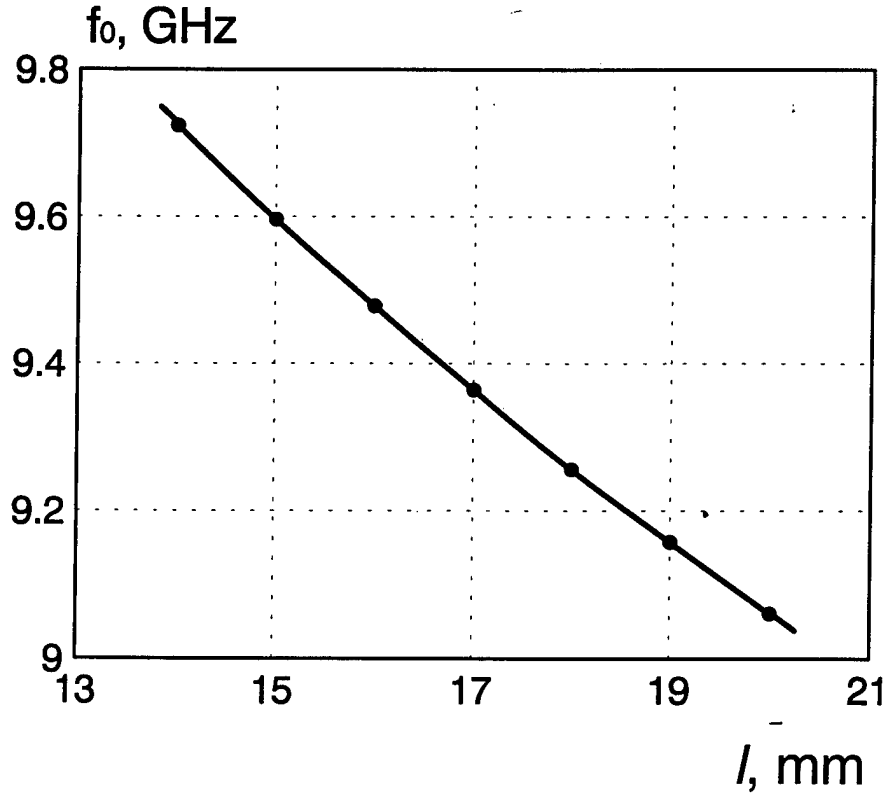

Fig. A3.2. Central frequency of the pass band vs
the filter micrometer screw position